ACS APPLIED MATERIALS & INTERFACES

Research Article

www.acsami.org

Steric Spacing of Molecular Linkers on Passivated Si(111) Photoelectrodes

Feng Li, Victoria M. Basile, Ryan T. Pekarek, and Michael J. Rose*

Department of Chemistry, The University of Texas at Austin, Austin, Texas 78712-1224, United States

Supporting Information

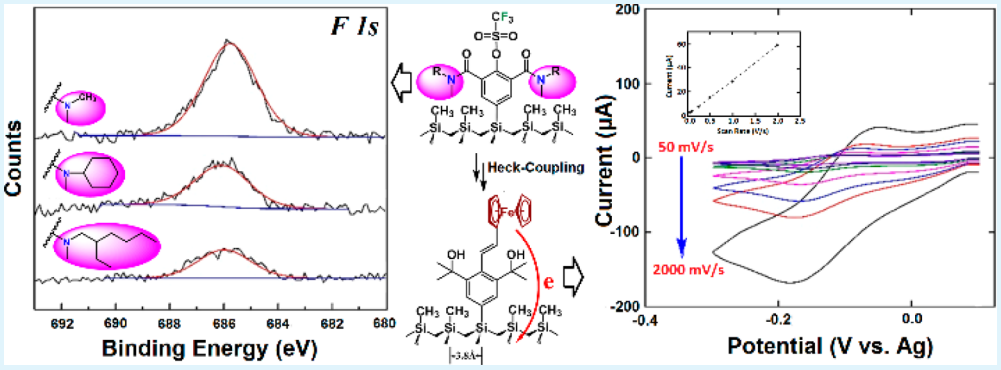

ABSTRACT: Surfaces with high photoelectrochemical and electronic quality can be prepared by tethering small molecules to single-crystalline Si(111) surfaces using a two-step halogenation/alkylation method (by Lewis and co-workers).[1−7] We report here that the surface coverage of custom-synthesized, phenyl-based molecular linkers can be controlled by varying the steric size of R-groups (R = CH_3, C_6H_{11}, 2-ethylhexyl) at the periphery of the linker. Additionally, the linkers possess a para triflate group ($-O_2SCF_3$) that serves as a convenient analytical marker and as a point of covalent attachment for a redox active label. Quantitative X-ray photoelectron spectroscopy (XPS) measurements revealed that the surface coverage systematically varies according to the steric size of the linker: CH_3 (6.7 ± 0.8%), CyHex (2.9 ± 1.2%), EtHex (2.1 ± 0.9%). The stability of the photoelectrochemical cyclic voltammetry (PEC-CV) behavior was dependent on an additional methylation step (with CH_3MgCl) to passivate residual Si(111)−Cl bonds. Subsequently, the triflate functional group was utilized to perform Pd-catalyzed Heck coupling of vinylferrocene to the surface-attached linkers. Ferrocene surface coverages measured from cyclic voltammetry on the ferrocene-functionalized surfaces Si(111)−**8a**/CH_3−Fc (R = CH_3) and Si(111)−**8c**/CH_3−Fc (R = 2-EtHex) are consistent with the corresponding Fe 2p XPS coverages and suggest a ∼1:1 conversion of surface triflate groups to vinyl-Fc sites. The surface defect densities of the linker/CH_3 modified surfaces are dependent on the coverage and composition of the organic layer. Surface recombination velocity (SRV) measurements indicated that *n*-Si(111)−**8a**/CH_3 and the ferrocene coupled *n*-Si(111)−**8a**/CH_3−Fc exhibited relatively high surface carrier lifetimes (4.51 and 3.88 μs, respectively) and correspondingly low *S* values (3880 and 4510 cm s^{-1}). Thus, the multistep, linker/Fc functionalized surfaces exhibit analogously low trap state densities as compared to the fully passivated *n*-Si(111)−CH_3 surface.

KEYWORDS: *Si(111), surface functionalization, passivation, steric spacing, photoelectrochemistry, covalent attachment*

INTRODUCTION

Silicon substrates have attracted tremendous attention for over half of a century because of their broad impact on the development of computing platforms, photovoltaics and nanoscale devices. The semiconductor industry relies heavily on the construction of layered materials on Si or SiO_x surfaces for microelectronics,[8−11] photoelectrochemistry or photocatalysis,[12−15] and chemical or biochemical sensors.[16−19] As silicon devices continue to be miniaturized to the nanoscale, the higher ratio of surface area to bulk Si has an increasingly important impact on device properties and performance. It is thus necessary to consider surface modifications or passivation strategies to optimize performance and longevity. Such functionalization (via materials chemistry or molecular modification) can allow for robust chemical passivation of the substrate. The attachment of functional monolayers onto silicon surfaces is intended to broaden the chemical, physical and electronic properties of the material.[20]

A number of methods have been developed to prepare functional monolayers on silicon surfaces, which can be attached by both covalent and noncovalent means. Formation of molecular layers on crystalline silicon surfaces without an intervening oxide layer is an extremely appealing approach toward robust layers on a surface. Chidsey reported the

Received: September 11, 2014
Accepted: October 29, 2014
Published: October 29, 2014

formation of monolayers composed of long chain alkyl groups covalently attached to silicon surfaces without an intervening oxide layer to result in an oxygen free surface,[21] as required for practical applications without leakage currents.[22] It is known that an H-terminated Si(111) single-crystalline surface has a low defect-state density that results in high electronic quality and good interfacial electron-transfer properties when in contact with liquid electrolytes that contain outer-sphere redox couples.[23,24] However, this surface is susceptible to oxidation within seconds to minutes upon exposure to air and/or moisture.[2,25−27] The facile degradation of the H-terminated Si(111) surface thus renders it unsuitable for direct use in many devices, including aqueous sensing applications or prolonged photoelectrochemical experiments.

The uniformly oriented bonding geometry of the Si(111) crystalline face is another unique aspect of this surface. Three bonds of each atop silicon tetrahedron are directed down into the bulk silicon, whereas the fourth bond is perpendicular to the plane of the surface. This apical Si site is thus available for chemical functionalization. Several approaches have been developed to stabilize the H-terminated Si(111) single-crystalline surface, including functionalization with Si−O−C self-assembled monolayers (SAMs)[28,29] or modifying the surface with Si−C,[6,30−33] Si−S[34] and Si−N[35,36] bonds to provide a chemically and thermally robust surface. The functionalization of H-terminated silicon surfaces with Si−C bonds, in particular, not only prevents the formation of an insulating SiO_2 oxide layer[37−40] but also provides an electronically coupled interface between the bulk semiconductor and a metal[41,42] or solution[43] without the interference of an interfacial oxide barrier.[37,44−46]

However, Si−C modifications have been limited by commercially available reagents, such as sources of methyl, ethyl, allyl, phenyl, thienyl and other various alkyl groups. These units often do not provide high surface coverage (inferior passivation), and lack heteroatom markers for facile quantification of surface coverage by X-ray photoelectron spectroscopy (XPS). Perhaps more importantly, most of the aforementioned groups are not amenable to secondary functionalization, thus limiting the chemical utility of the prepared surfaces. Some exceptions must be noted, such as reports detailing the bromination of the thienyl and allyl moieties, and their subsequent reactivates.[32] It would be advantageous to retain precise synthetic control over the organic structures at the interface, so that new chemical functionality can be tailored to meet predefined physical or chemical requirements.

A rendering of the Si(111) crystal face reveals a hexagonal array of atop Si atoms, wherein the spacing between atop sites is ∼3.84 Å. Therefore, the surface modification to an atop silicon site is largely governed by the steric size of the intended attachment moiety. For example, small groups like methyl (d = 3 Å) achieve ∼100% coverage.[6] By the same reason, surface coverage is always decreased as the size of the molecules increase. For example, attachment of phenyl groups afford a maximum coverage of ∼50%,[7] and even larger organic moieties such as benzoquinone achieve less than 10% coverage.[47] The residual sites remain chemically unpassivated, which leads to undesirable formation of silicon oxide and surface defects. To eliminate this issue, Lewis and co-workers have shown that the smaller methyl groups can be utilized to "in-fill" the unoccupied sites, as methyl groups provide >95% passivation on the unreconstructed Si(111) surface.[31,32,48,49]

For novel applications in energy conversion, it would be desirable to incorporate more complex organic moieties to control both surface coverage and surface functionality. In our work, we are interested in providing a rational design element to control the coverage of functional linker moieties on the Si surface. Although methyl group passivation does provide high electronic-quality surfaces that are generally inert to oxidation, it lacks any useful functionality for secondary attachment of molecules or interfacial interaction with materials (heterojunction). Indeed, the secondary attachment of redox-driven catalysts or molecular sensing moieties would require a linker moiety that would facilitate fast electron transfer and/or electronic communication between bulk Si and the active interface. The inert, hydrophobic surface of the conformal Si(111)−CH_3 monolayer does not provide an ideal interface for contacting other materials, such as the metal oxides or metal films used in electronics, photovoltaics or the developing field of solar fuels devices. Herein we report surface modification on Si(111) with phenyl-based, diamide linkers with different molecular diameters. The modified substrates were investigated using a variety of characterizations including X-ray photoelectron spectroscopy (XPS), photoelectrochemical cyclic voltammetry (PEC-CV) and contact angle goniometry. To show the chemical functionality of the surface, as well as to provide a second method of surface coverage quantification, we utilized Heck coupling to covalently attach a vinylferrocene redox moiety to the linker sites. The advantages of controlling the surface coverage at the molecular level are discussed.

EXPERIMENTAL SECTION

Chemicals and Materials. *n*-Type Si(111) oriented wafers (Cz grown, single-side polished, 350 μm thickness, 1−10 Ω·cm) were purchased from Virginia Semiconductor. Etching procedures were performed using buffered $HF_{(aq)}$ and 11 M $NH_4F_{(aq)}$ (semiconductor grade, Transene). The following chemicals were used as received: 4-bromo-2,6-dimethylphenol and phosphorus pentachloride (Alfa Aesar); methyl iodide, di-*tert*-butyl dicarbonate, lithium aluminium hydride, dimethylamine and 2.5 M *n*-butyllithium solution in hexane (Acros Organics); thionyl chloride, 1.0 M boron tribromide solution in CH_2Cl_2, sodium hydride, *N*-phenyl-bis(trifluoromethanesulfonimide), anhydrous chlorobenzene, benzoyl peroxide and vinylferrocene (Sigma-Aldrich); 2-ethylhexylamine (Tokyo Chemical Industry Co, Ltd.); tetrakis(triphenylphosphine) palladium(0) (Strem Chemicals). All solvents were purchased as high-performance liquid chromatography (HPLC)-grade and purified over alumina with a Pure Process Technology solvent purification system. Nanopure deionized water having a resistivity of 18 MΩ·cm or higher (Barnstead Nanopure Systems) was used in all procedures involving wafer surfaces.

Characterization of Organic Intermediates and Linkers. The ^1H, ^{13}C and ^{19}F NMR spectra were measured on a VARIAN Direct Drive NMR spectrometer (400 MHz), and ^1H chemical shifts are reported as δ values in ppm vs TMS. IR spectra were measured on a Bruker ALPHA Fourier transform infrared (FTIR) spectrometer equipped with a diamond ATR crystal. Mass spectrometry (MS) data were measured with an Agilent Technologies 6530 Accurate Mass QTofLC/MS.

Synthesis of Diamide Triflates (8; Scheme 1). *N-Methyl-2-ethylhexylamine (2).* The liquid 2-ethylhexylamine (645 mg, 5.0 mmol) was diluted in 25 mL of dry THF. Di-*tert*-butyl dicarbonate (1.31 g, 6.00 mmol) was slowly added to the mixture at room temperature and stirred overnight to form *tert*-butyl hexylcarbamate (**1**) in the mixture. Then, $LiAlH_4$ (1.14 g, 30.0 mmol) was added to the reaction mixture over the course of 1 h, and the mixture was heated to reflux temperature overnight. The reaction mixture was cooled to room temperature and filtered. Due to the volatility of the product, the THF solution of the product was used directly in the

Scheme 1. Synthesis of Phenyl Triflate Diamides

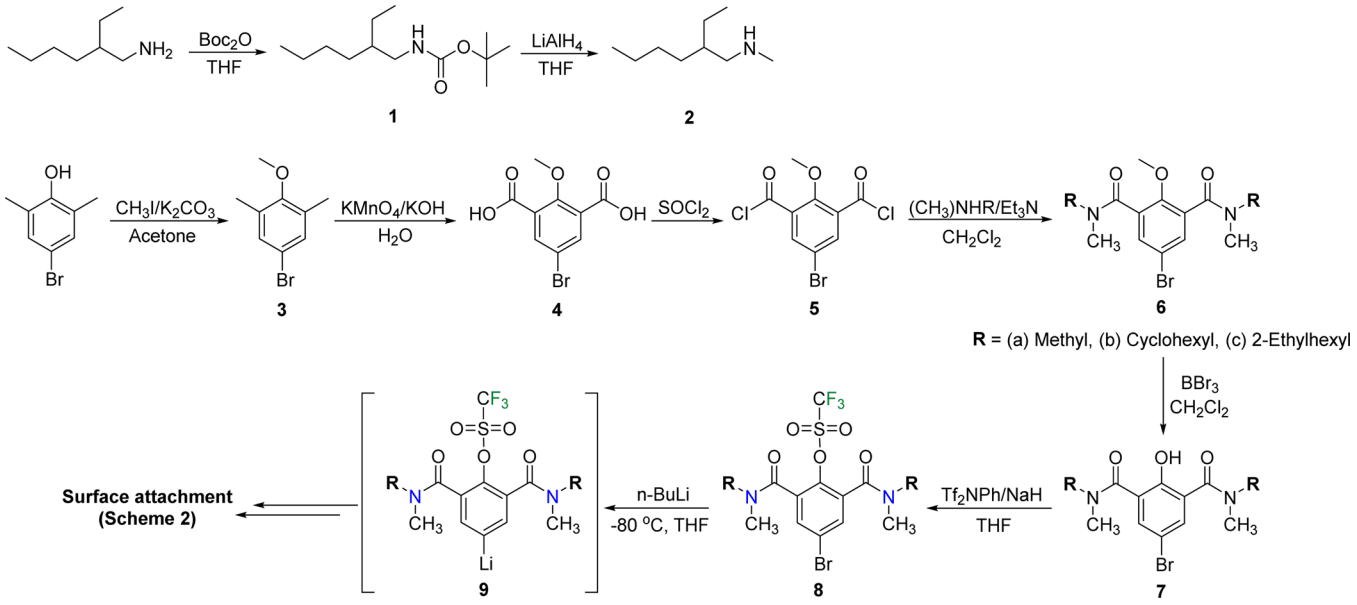

subsequent reaction. ^{1}H NMR (400 MHz, $CDCl_3$): δ 2.46 (d, 2H), 2.42 (s, 3H), 1.50−1.20 (m, 9H), 0.98 (s, 1H), 0.89 (t, 3H), 0.86 (t, 3H). ^{13}C NMR ($CDCl_3$): δ 55.2, 39.0, 36.4, 31.6, 28.7, 24.1, 22.7, 13.6, 10.4.

*2,6-Dimethyl-4-bromoanisole (**3**).* A small batch of 2,6-dimethyl-4-bromophenol (328 mg, 1.63 mmol) was dissolved in 5 mL of acetone, then 0.31 mL of MeI (700 mg, 4.92 mmol) and K_2CO_3 (460 mg, 3.33 mmol) were added to the solution. The reaction mixture was heated at reflux temperature overnight and then the solvent was evaporated under vacuum. The residue was dissolved in ethyl acetate (30 mL), washed with saturated $NaHCO_3$ (3 × 30 mL) and brine (3 × 30 mL) and then dried over Na_2SO_4. The solvent was evaporated to give a yellow oil. Hexane was used for chromatography, to afford a colorless oil as product. Yield: 280 mg (80.0%). ^{1}H NMR (400 MHz, $CDCl_3$): δ 7.14 (s, 2H), 3.69 (s, 3H), 2.25 (s, 6H). ^{13}C NMR ($CDCl_3$): δ 156.1, 133.1, 131.4, 116.3, 59.7, 15.9.

*2,6-Dicarboxyl-4-bromo-anisole (**4**).* The product above (**3**) 2,6-dimethyl-4-bromo-anisole (280 mg, 1.30 mmol) was mixed with 20 mL of water, KOH (32 mg) and $KMnO_4$ (820 mg), then heated to reflux temperature overnight. The mixture was filtered and the solid was washed with a small amount of 2 M KOH. Concentrated HCl was slowly added to the filtration until the pH approached ∼2. A white precipitate was obtained, collected by filtration, washed with water and dried under vacuum to afford the product as a white solid. Yield: 229 mg (63.9%). ^{1}H NMR (400 MHz, DMSO): δ 13.43 (s, 1H), 7.92 (s, 2H), 3.78 (s, 3H). ^{13}C NMR (DMSO): δ 166.0, 157.2, 135.9, 130.4, 115.5, 63.6.

*5-Bromo-2-methoxy-N^1,N^1,N^3,N^3-tetramethylisophthalamide (**6a**).* A batch of (**4**) 2,6-dicarboxyl-4-bromo-anisole (220 mg, 0.800 mmol) was mixed with 4.4 mL of $SOCl_2$ and heated to reflux temperature. After the white solid dissolved to completion, the mixture was refluxed for another 30 min, then the excess $SOCl_2$ was evaporated under vacuum. The white solid residue was dried under high vacuum for 3 h. The residue was dissolved in CH_2Cl_2, then 0.8 mL of a stock 2 M solution of dimethylamine in THF was added at 0 °C followed by 0.3 mL of triethylamine. The mixture was stirred overnight at room temperature, filtered (to remove NEt_3·HCl), and the solvent was removed under vacuum. Chromatography on silica gel with ethyl acetate as the mobile phase provided a white solid as the product. Yield: 186 mg (70.7%). ^{1}H NMR (400 M Hz, $CDCl_3$): δ 7.39 (s, 2H), 3.79 (s, 3H), 3.11 (s, 6H), 2.88 (s, 6H). ^{13}C NMR ($CDCl_3$): δ 167.1, 151.3, 131.6, 38.4, 34.9.

*5-Bromo-N^1,N^3-dicyclohexyl-2-methoxy-N^1,N^3-dimethylisophthalamide (**6b**).* This product was also prepared from **4** per the procedure for **6a**, and isolated as a white solid. Yield: 292 mg (68.1%). ^{1}H NMR (400 MHz, $CDCl_3$): δ 7.34 (s, 2H), 3.78 (s, 3H), 2.96 (m, 2H), 2.71 (s, 6H), 1.90−0.90 (m, 20H). ^{13}C NMR ($CDCl_3$): δ 166.7, 150.8, 133.9, 131.0, 117.0, 58.6, 52.7, 30.6, 29.6, 25.6, 25.1.

*5-Bromo-N^1,N^3-di(2-ethylhexyl)-2-methoxy-N^1,N^3-dimethylisophthalamide (**6c**).* This product was also prepared from **4** per the procedure of **6a**, and isolated as a white solid. Yield: 412 mg (60.4%). ^{1}H NMR (400 MHz, $CDCl_3$): δ 7.53 (s, 2H), 3.73 (s, 3H), 3.62 (d, 4H), 2.33 (s, 6H), 1.70−0.80 (m, 30H). ^{13}C NMR ($CDCl_3$): δ 167.3, 150.9, 132.2, 132.0, 131.1, 54.6, 50.7, 37.0, 30.4, 28.7, 23.7, 23.1, 14.1, 10.5.

*5-Bromo-2-hydroxy-N^1,N^1,N^3,N^3-tetramethylisophthalamide (**7a**).* The product from the above procedure **6a** (186 mg, 0.57 mmol) was dissolved in 10 mL of CH_2Cl_2 and cooled −78 °C. Next, 1.5 mL of BBr_3 in THF (1 M) was added to the mixture dropwise, and the temperature was allowed to increase to room temperature with continued stirring for 3 h. The reaction was quenched with 5 mL of water and diluted with 30 mL of ethyl acetate. The organic phase was washed with brine (2 × 30 mL) and dried over Na_2SO_4. The solvent was evaporated, and ethyl acetate through a silica gel flash chromatography column afforded the product as a yellow solid. Yield: 170 mg (95.5%). ^{1}H NMR (400 MHz, $CDCl_3$): δ 10.35 (s, 1H), 7.45 (s, 2H), 3.09 (s, 12H). ^{13}C NMR ($CDCl_3$): δ 168.4, 154.4, 132.7, 123.7, 110.1, 37.6.

*5-Bromo-N^1,N^3-dicyclohexyl-2-hydroxy-N^1,N^3-dimethylisophthalamide (**7b**).* This product was prepared from **6b** per the procedure for **7a**, and isolated as a white solid. Yield: 248 mg (91.8%). ^{1}H NMR (400 MHz, $CDCl_3$): δ 10.09 (s, 1H), 7.37 (s, 2H), 4.02 (m, 2H), 2.92 (s, 6H), 1.80−1.00 (m, 20H). ^{13}C NMR ($CDCl_3$): δ 168.2, 154.1, 131.9, 124.6, 110.1, 60.4, 56.2, 30.1, 25.5, 25.4.

*5-Bromo-N^1,N^3-di(2-ethylhexyl)-2-hydroxy-N^1,N^3-dimethylisophthalamide (**7c**).* This product was prepared from **6c** per the procedure for **7a**, and isolated as a yellow oil. Yield: 362 mg (93.1%). ^{1}H NMR (400 MHz, $CDCl_3$): δ 10.00 (s, 1H), 7.41 (s, 2H), 3.38 (m, 4H), 3.03 (s, 6H), 1.70−0.80 (m, 30H). ^{13}C NMR ($CDCl_3$): δ 168.7, 153.9, 132.4, 110.1, 37.1, 30.3, 28.6, 23.5, 23.0, 14.1, 10.5.

*4-Bromo-2,6-bis(dimethylcarbamoyl)phenyl trifluoromethanesulfonate (**8a**).* To a mixture of 19 mg NaH in 10 mL of dry THF was added 170 mg (0.54 mmol) of **7a** in 3.4 mL of dry THF at 0 °C, followed by the addition of 202 mg (0.56 mmol) of *N*-phenyl-bis(trifluoromethanesulfonimide) in 4 mL of dry THF. The mixture was stirred for 30 min and then heated for 4 h at reflux. The reaction was quenched with 20 mL of water and extracted with 30 mL of CH_2Cl_2. The organic phase was washed with water (20 mL) and brine (20 mL) and then dried over Na_2SO_4. After evaporation, the residual

dx.doi.org/10.1021/am506244m | ACS Appl. Mater. Interfaces 2014, 6, 20557−20568

Scheme 2. Surface Modification Procedures for Linker Attachment, Passivation and Coupling of the Vinylferrocene Redox Marker

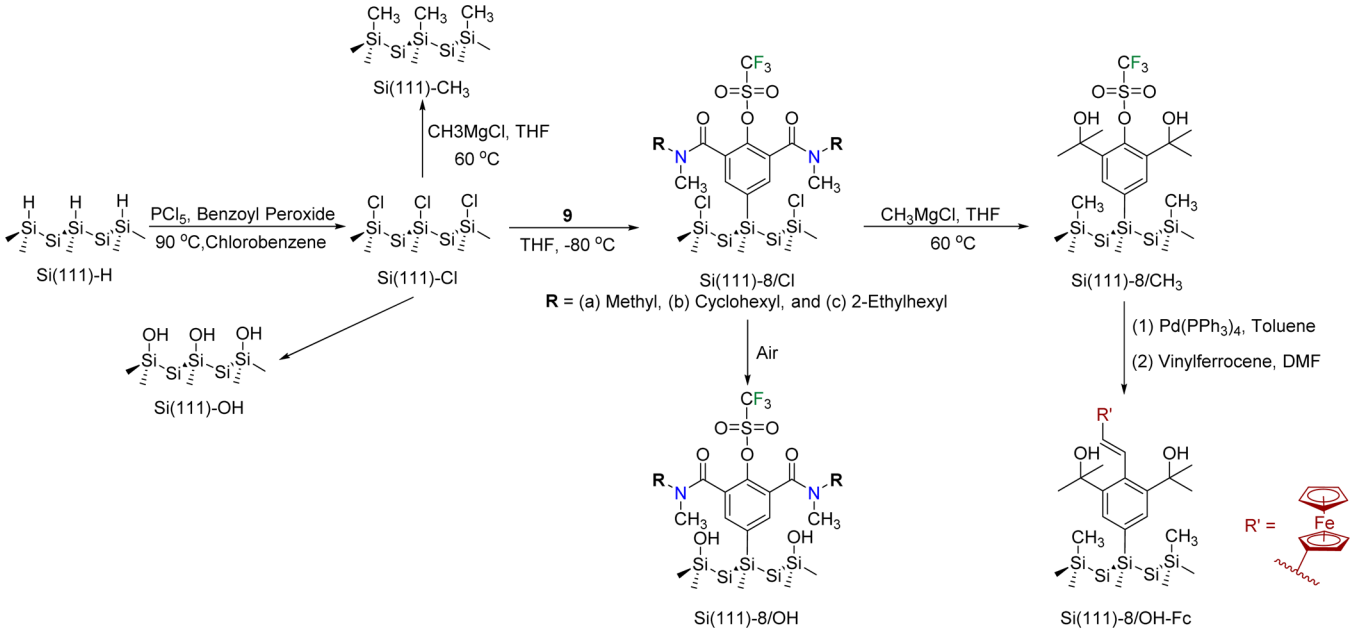

oil was chromatographed on silica gel (first CH_2Cl_2, then EtOAc) to yield the product as a white solid. Yield: 175 mg (72.6%). ^{1}H NMR (400 MHz, $CDCl_3$): δ 7.58 (s, 2H), 3.09 (s, 6H), 2.94 (s, 6H). ^{13}C NMR ($CDCl_3$): δ 163.9, 139.5, 133.4, 132.7, 122.4, 119.8, 38.7, 35.0. ^{19}F NMR: δ 73.84. FTIR (cm^{-1}): 3087, 2937, 1642, 1414, 1390, 1202, 1140, 1069, 897, 806, 728, 602. HRMS (ESI): m/z calculated for $C_{13}H_{14}BF_3N_2O_5S$ (M + H), 446.9832; found, 446.9958.

*4-Bromo-2,6-bis(cyclohexyl(methyl)carbamoyl)phenyl trifluoromethanesulfonate (**8b**).* This product was prepared from **7b** per the procedure for **8a**, and isolated as a white solid. Yield: 208 mg (68.5%). ^{1}H NMR (400 MHz, $CDCl_3$): δ 7.50 (s, 2H), 4.45 (m, 1H), 3.25 (m, 1H), 2.96 (s, 3H), 2.79 (s, 3H), 1.80−1.00 (m, 20H). ^{19}F NMR: δ 73.8. ^{13}C NMR ($CDCl_3$): δ 167.6, 163.6, 134.3, 132.4, 122.2, 58.9, 53.4, 37.8, 31.4, 30.3, 27.5, 25.5. ^{19}F NMR: δ 73.33. FTIR (cm^{-1}): 3520, 3464, 3051, 2960, 1620, 1407, 1205, 1139, 1104, 893, 606. HRMS (ESI): m/z calculated for $C_{23}H_{30}BF_3N_2O_5S$ (M + H), 583.1084; found, 583.1091.

*4-Bromo-2,6-bis(2-ethylhexyl(methyl)carbamoyl)phenyl trifluoromethanesulfonate (**8c**).* This product was prepared from **7c** per the procedure for **8a**, and isolated as a colorless oil. Yield: 358 mg (81.4%). ^{1}H NMR (400 MHz, CDCl3): δ 7.49 (s, 2H), 3.03 (d, 6H), 2.90 (d, 4H), 1.80−0.60 (m, 30H). ^{13}C NMR ($CDCl_3$): δ 169.6, 164.7, 134.2, 133.8, 133.6, 132.4, 129.5, 127.1, 123.3, 54.5, 51.3, 37.5, 37.2, 36.8, 33.1, 30.5, 23.1, 14.1. ^{19}F NMR: δ 73.49. FTIR (cm^{-1}): 2959, 2928, 2860, 1645, 1459, 1209, 1136, 872, 801, 728, 648, 610, 572. HRMS (ESI): m/z calculated for $C_{27}H_{42}BF_3N_2O_5S$ (M + H), 643.2023; found, 643.2029.

Preparation and Surface Treatment of Silicon Substrates (see Scheme 2). *Oxidation and Removal of Organic Contaminants from Si Surfaces.* Si(111) wafers were cut to the desired size and then rinsed with water, methanol and acetone. The samples were dried under a stream of N_2. Hot piranha acid (1:3, 30% $H_2O_{2(aq)}$/18 M H_2SO_4, 90 °C for 10 min) was used to remove surface organic contaminants. ***Caution***: Piranha solution is aggressive and explosive. Never mix piranha waste with solvents. Check the safety precautions before using it. The wafers were then rinsed with copious amounts of water and dried under N_2. The samples were HF-etched immediately after cleaning with the Piranha solution.

Anisotropic Etching to Form Atomically Flat Si(111)−H.[32] Si(111) samples were submerged for 10 s in buffered $HF_{(aq)}$. The solution was drained, and excess HF was rinsed away with water. The substrates were submerged for 20 min in an 11 M $NH_4F_{(aq)}$ solution that was previously degassed by bubbling with N_2 for 30 min. During submersion, the samples were agitated occasionally to remove bubbles from the surface of the wafer. They were then removed from the NH_4F solution, rinsed thoroughly with water and dried under a stream of $N_{2(g)}$. Within several minutes of etching, the freshly prepared Si(111) surfaces were introduced into a N_2 atmosphere glovebox.

Preparation of Chlorine-Terminated Si(111) Surface. The chlorine-terminated Si(111) surface was prepared by a previously described procedure using PCl_5.[3] A solution of PCl_5, in chlorobenzene solvent with a trace amount of benzoyl peroxide as a reaction initiator, was added to a hydrogen-terminated Si(111) wafer in an inert atmosphere glovebox. The entire reaction was placed in an oil bath at 90 °C for 1 h. The chlorine-terminated surface was removed from the solution and rinsed with dry chlorobenzene and THF.

Surface Functionalization and Passivation of Chlorine-Terminated Si(111) Surface. The desired bromophenyl linker was placed under N_2 in 5 mL of anhydrous THF and cooled to −80 °C. To this stirred solution was added 0.9 equiv of 1.6 M *n*-BuLi in hexanes and the linker was allowed to lithiate for 30 min (**9** in Scheme 1). The chlorine-terminated Si(111) samples were transferred from the glovebox into this solution quickly while maintaining the temperature at −80 °C. The solution was slowly warmed up to 0 °C over a 1 h period. Samples that underwent subsequent methylation were subjected to the following procedure: substrates were transferred back to the glovebox and treated with a 1.0 M CH_3MgCl solution in THF at 60 °C for 30 min, according to the published procedure.[32] When all surface functionalizations were completed, the wafers were washed with THF, MeOH and H_2O, followed by sonication for 10 min in each solvent to remove any noncovalently attached species.

Pd Addition and Heck Coupling.[32] Si(111) substrates were first functionalized with the diamide triflate linkers and exposed to the methylation procedure to achieve surface passivation. The wafers were then exposed to a solution of 5 mg/mL of [$Pd(PPh_3)_4$] in toluene for 1 h at room temperature. The Pd-activated samples were then rinsed thoroughly with toluene, followed by a rinse with DMF. The samples were then submerged into a 0.5−0.8 M DMF solution of vinylferrocene. The reaction mixture was sealed in a pressure vessel, and the vessel was wrapped in foil to prevent exposure to light and heated to 100 °C for 30 min. The reaction mixture was cooled and then opened to air. The silicon surfaces were rinsed sequentially with water, methanol, acetone, methanol and water.

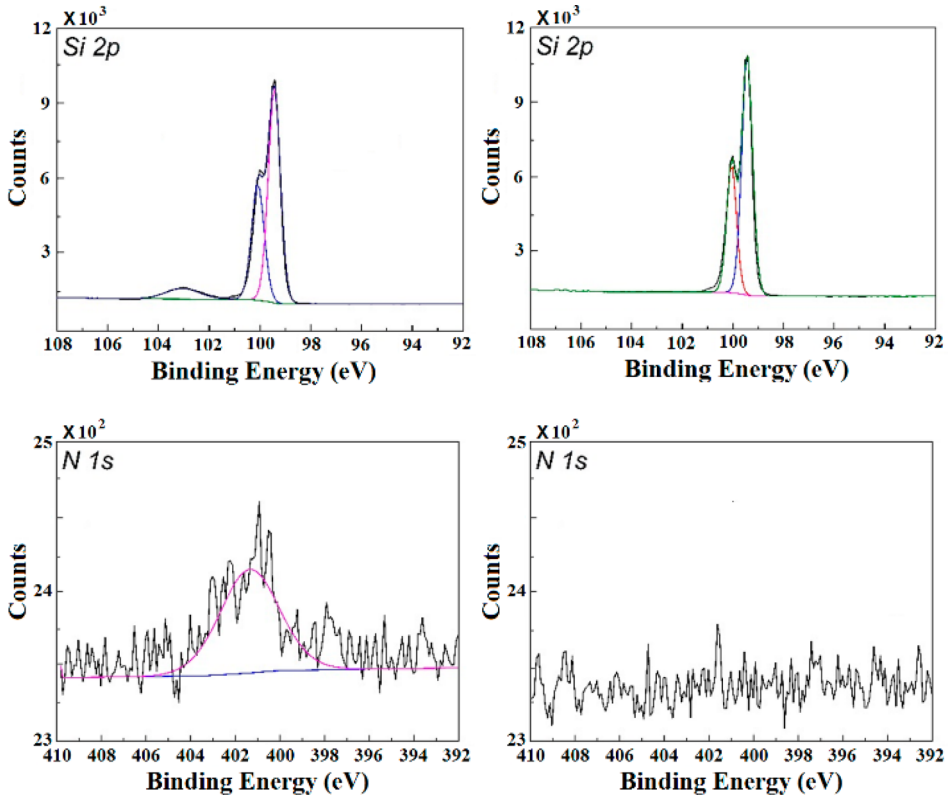

Figure 1. High-resolution Si 2p and N 1s X-ray photoelectron spectra of **8c** modified substrates without methylation (left) or with methylation (right).

Surface Characterization Methods. X-ray photoelectron spectroscopy (XPS) data was collected using a Kratos Axis Ultra XPS. Hydrophobicity was determined by water contact angle on modified surface Si(111) samples using a contact angle goniometer (Model 100-00-115, Rame Hart, Netcong, NJ) by reading contact angle values of the two sides of a drop (2 μL) within 30 s after deposition of the drop. The average water contact angle was calculated for the three individual samples at two different spots. Electrochemical measurements were carried out using a functionalized Si(111) substrate as the working electrode (electrode area: 0.44 cm^2, defined by the O-ring between working electrode and electrolyte), a Pt wire counter electrode and a Ag wire reference electrode; 60 mM ferrocene was used as the redox couple in 1 M $LiClO_4/CH_3CN$ solution in a one-compartment cell. Substrates were illuminated with an Oriel 150 W light source fitted with an AM 1.5 filter, with an intensity at the sample of 100 mW/cm^2 (1 sun). Dark measurements were performed as control for each substrate (<1 μA dark current). Cyclic voltammetry data was obtained using a Pine Wavenow potentiostat driven by AfterMath software v1.2.5033. Surface recombination velocities were obtained using a microwave conductivity apparatus equipped with an IR laser, as purchased from Growth Equipment, Inc.

RESULTS AND DISCUSSION

A. Synthesis and Rationale. Previous studies have shown that atop coverage of organic moieties varies roughly according to the size of the target passivation agent. For example, while methyl groups can attain essentially 100% occupancy on Si atop sites (3.84 Å spacing), larger groups such as ethyl, phenyl or thienyl exhibit lower maximum coverages (90 ± 20%, 50 ± 20% and 55 ± 8%, respectively).[5,7] Ultimately, we seek to provide two major improvements to the existing body of work: (i) obtain precise control over surface coverages as determined by steric size and (ii) impart a higher level of chemical functionality on the surface through synthetic means. To achieve the first aim, we sought to synthetically control the steric size of molecular linkers on a single framework to rationally modulate their coverage on the Si(111) surface. The choice of R groups flanking the phenyl-diamide linker ranged from smallest (CH_3, $d \approx 3$ Å) to largest (2-ethyl-hexyl) as shown in Scheme 1. Although long chain spacers like *n*-hexyl were considered, straight chain moieties can often lead to higher than expected surface coverages due to their high flexibility (i.e., can point "up" instead of across the wafer) and their ability to conform into high density self-assembled monolayers.[7,50] As our goal in this work was to maximize the range of surface coverages, we opted for the 2-ethylhexyl moiety, which is known to be sterically large and to exhibit low packing density due to the irregular shape of its 2-ethyl branch.

To generate the target family of phenyl-triflate-diamide linkers, we first attempted $KMnO_4$ oxidation of the triflate-protected *p*-bromo-2,6-dimethylphenol (not shown). However, separation of triflate dicarboxylates from the aqueous layer proved difficult, and thus a more involved protection/deprotection sequence was required. Oxidation of the methylated *p*-bromo-2,6-dimethylanisole (**3**, 80%) proceeded smoothly, and the compound was isolable from the reaction mixture. Subsequent activation with $SOCl_2$ and coupling with the selected methylamines produced the methoxy-protected diamides in good yields (60−70%). Subsequent methoxy deprotection with BBr_3 and installation of the triflate moiety with Tf_2NPh was straightforward and high-yielding, thus affording the target products.

B. Linker Attachment. Prior studies have achieved mixed monolayer compositions on Si(111) via two methods: (i) sequential addition of large reagents (R = phenyl-lithium, thienyl-lithium), followed by small reagents (CH_3MgCl) to in-

fill the unpassivated sites;[3,7,32,48] or (ii) simultaneous addition of large and small reagents in varying molar ratios to achieve the desired surface coverage of the larger moiety.[51] In this work, we chose the former approach due to the incompatibility of the phenyl-diamide linkers with the Grignard reagent. Prolonged incubation of the amides with CH_3MgCl will result in alkylation of the carbonyl moiety,[52] introducing the likelihood of linker transformation or decomposition prior to attachment (vide infra surface attachment, and Scheme 2).

Although this reactivity concern detracts from the available options to modulate surface coverage, it does provide additional functionality once the surface is modified with the linkers. As shown in Scheme 2, methylation after linker attachment (and MeOH wash) results in alkylation of the carbonyl (vide infra, XPS analysis). This should afford the corresponding phenyl(di-isopropyl alcohol) moieties that may modulate barrier height, anchor molecular attachments, or interface with metal oxide materials in further applications.

C. X-ray Photoelectron Spectroscopy Analyses of Functionalized Si(111) Surfaces. Figure 1 shows the high-resolution X-ray photoelectron spectra (XPS) of the Si 2p and N 1s regions for **8c** (R = 2-Et-Hex) functionalized Si(111) surfaces with and without additional methylation (right and left, respectively). A high-resolution scan of the Si 2p region for the surface without methylation revealed a significant feature at 102.9 eV, corresponding to ~1 monolayer of surface oxide from unmodified atop Si sites. This oxide layer is attributable to the presence of unpassivated surface Si−Cl sites, which rapidly oxidize to $Si-O_x$ in air. Notably, the high-resolution scan of the Si 2p region for the surface treated with methylating agent (CH_3MgCl) showed only the signal corresponding to bulk Si (2p, 100 eV). This suggests that the remaining unmodified Si−Cl sites have been covalently functionalized with CH_3, thus preventing oxidation by air.

The N 1s features were also compared for the **8c** functionalized Si(111) surface before and after methylation. The high-resolution spectrum of N 1s for **8c** functionalized Si(111) surface without methylation showed a peak centered at 401 eV, corresponding to ~4% of N atoms surface coverage. First, the binding energy of the N 1s is consistent with a δ^+(N) peak (e.g., NH_4^+ = 401 eV), as expected for the resonance stabilized nitrogen in the amide-enol unit. Second, the full width at half maximum (fwhm) of the N 1s peak in Figure 1 (bottom left) is ~2.8 eV, which is slightly broader than that of literature data for a homogeneous C−N bond (~2 eV). The observed broadening of the peak may be attributable to two factors: (i) the constitutional isomerism in the resonance structure described above, or (ii) the geometrical isomerism that results from rotation about the disubstituted $N-(R)_2$.

Following exposure of the substrate to methylmagnesium chloride in THF solution at 60 °C, the nitrogen signal was eliminated. As shown in Scheme 2, the substituted methyl-amides on the phenyl core will react with CH_3MgCl, resulting in cleavage of the diamide from the phenyl anchor during methylation. This finding illustrates the possibility regarding the hydrolysis/alkolysis or deprotection of spacer arms following attachment of the linkers. Such a scheme may prove useful in future applications.

The effect of varying R-group size was investigated by XPS analysis of the F 1s region (triflate marker). Figure 2 shows the X-ray photoelectron spectra for mixed **8**/methyl Si(111) surfaces. The survey spectra (Figure 2a) exhibited peaks corresponding to Si (2p, 100 eV), C (1s, 285 eV), O (1s, 532 eV) and F (1s, 686 eV). Quantitative analysis of the surface coverage was based on the F 1s signals. In this calculation, the fluorine signals were parametrized as arising from the triflate ($-SO_2CF_3$) markers on the linkers (three F atoms per linker). [Note: The N 1s features are not observed in the spectra due the amide alkylysis incurred by CH_3MgCl treatment.] Figure 2b shows the comparisons among the high-resolution X-ray photoelectron spectra of F 1s on **8a**, **8b** and **8c** functionalized mixed **8**/CH_3 Si(111) surfaces; in each case, there is an observable feature at 686 eV. Following quantification according to reported benchmarks,[5,7,32,48] the **8a**/CH_3 Si(111) surface exhibits a fluorine coverage value of 2.61 ± 3.30×10^{-10} mol/cm^2 corresponding to a linker coverage of 6.7 ± 0.8% of **8a** (Table 1) [by comparison, atop silicon is reported as 1.31×10^{-9} mol/cm^2].[7] Similarly, the **8b**/CH_3 and **8c**/CH_3

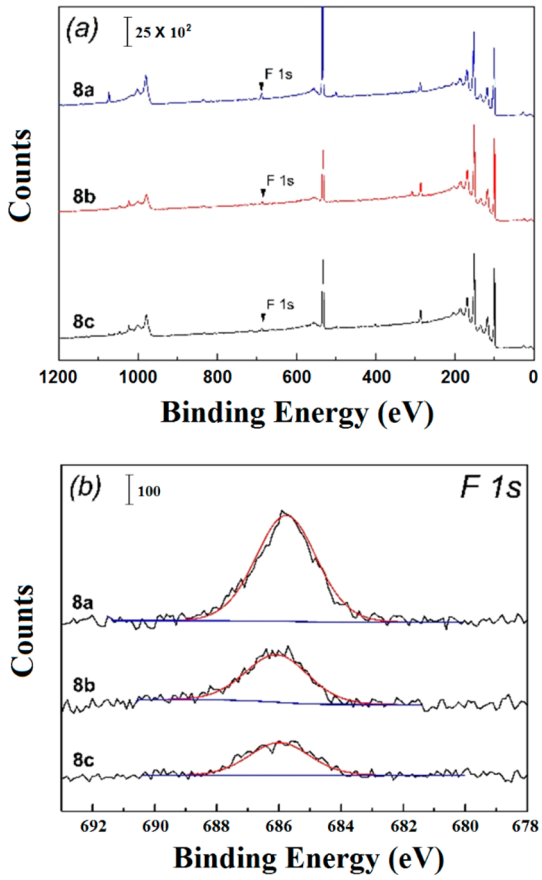

Figure 2. X-ray photoelectron spectra survey (a) and high-resolution F 1s (b) spectra of a series of **8**/CH_3−Si(111) surfaces.

Table 1. XPS and Electrochemical Surface Coverages for Organic Linkers (8a, 8b and 8c) and Heck-Coupled Ferrocene Samples

	coverage (%)		
	linker only	Fc-coupled	Fc-coupled
surfaces	XPS, F 1s[a]	E-chem, Fc[a]	XPS, Fe 2p[b]
Si(111)−**8a**/CH_3	6.7 ± 0.8	4.5 ± 0.6	4.2
Si(111)−**8b**/CH_3	2.9 ± 1.2	n/d	n/d
Si(111)−**8c**/CH_3	2.1 ± 0.9	1.8 ± 0.7	1.4

[a]Average ± standard deviation from three spots. [b]Fc-coupled XPS from one sample.

Si(111) surfaces exhibit linker coverages of 2.9 ± 1.2% and 2.1 ± 0.9%, respectively. Thus, the triflate-based XPS data indicates that the surface coverage of the molecular linkers is controlled by varying the steric size of the substituted methylamides (R = CH_3, cyclohexyl, 2-ethylhexyl; Scheme 1).

D. Water Contact Angle Measurements. Table 2 summarizes the water contact angle values (θ^{water}) of Si(111) substrates with various surface functionalization (Scheme 2). Beginning with the NH_4F etched Si(111), the atomically flat Si(111)−H results in a hydrophobic surface shown by a large water contact angle (99 ± 6°).[53,54] Subsequently, the silicon is slowly oxidized to yield a hydrophilic Si−O_x layer on the surface, resulting in the decrease of the contact angle (θ^{water} ≈ 56.2 ± 1.7°). As shown in Table 2, the methylated surface [Si(111)−CH_3] exhibits a high water contact angle (θ^{water}) of 110.8 ± 0.8°, indicating a very hydrophobic surface. According to previous studies, the formation of Si−C bonds inhibits the rate of oxidation;[45,55] therefore, the functional organic monolayers will not be susceptible to oxidation.[53,56]

Table 2. Water Contact Angle (deg) of Chemically Modified Si(111) Surfaces

surfaces	water contact angle, θ^{water} (deg)[a]
Si(111)−OH	56.2 ± 1.7
Si(111)−H	99 ± 6[b]
Si(111)−CH_3	110.8 ± 0.8
Si(111)−**8a**/OH	77.9 ± 2.9
Si(111)−**8b**/OH	71.1 ± 2.0
Si(111)−**8c**/OH	68.8 ± 4.6
Si(111)−**8a**/CH_3	95.6 ± 1.4

[a]Average ± standard deviation from three separate samples, two different spots for each sample. [b]Value from ref 54.

The water contact angles (θ^{water}) for the Si surfaces functionalized with the phenyl-based molecular linkers (**8a**−**c**) are less than the methylated surface [Si(111)−CH_3], but greater than the oxidized unmodified surface [Si(111)−OH]. For the **8a**/OH samples, the contact angle is smaller compared to the Si(111)−CH_3 surface due to the unmodified Si sites that are oxidized after exposure to air. The water contact angles decrease as the size of the substituted methylamides increases in the order of CH_3 (**8a**), C_6H_{11} (**8b**), 2-ethylhexyl (**8c**). The reason is likely that the decrease in Si-linker coverage causes a concomitant increase in SiO_x (or Si−OH) coverage, thus rendering the surface more hydrophilic. Notably, the additional methylation process on Si(111)−**8a** surface significantly increased the water contact angle from 77.9 ± 2.9 to 95.6 ± 1.4°, due to nearly complete termination of Si−Cl bonds with Si−CH_3 units (minimal Si−O_x/Si−OH). However, this contact angle is still smaller than the value obtained for Si(111)−CH_3 surface, possibly because the methylation process on Si(111)−**8a** surface incidentally provides two isopropyl−OH on each linker (Scheme 2). These interpretations are consistent with XPS data as shown in the last section.

E. Photo/Electrochemistry. *Stability by Methylation.* The redox activity and stability of the functionalized Si(111) surface was investigated by photoelectrochemical cyclic voltammetry (PEC-CV) under 1 sun illumination (AM1.5, 100 mW cm^{-2}). Substrates (*n*-Si) functionalized with **8a** and with or without methylation were subjected to 30 redox cycles at 250 mV/s in the presence of ferrocene (Fc) as an outer-sphere redox agent (1 mM, MeCN, 1.0 M $LiClO_4$). This experiment resulted in diffusion-limited, Nernstian CV waves for both samples (Figure 3). The anodic response was observed near −0.1 V vs Ag, followed by a cathodic response centered near −0.3 V vs Ag. The observed cathodic shift relative to the standard value for Fc in MeCN (about +0.18 V vs Ag in our cell) is due to the intrinsically anodic bias of illuminated *n*-type silicon. No peak currents were observed using the same photoelectrode under dark conditions (<10 μA). The relatively large ΔE_p value (~200 mV) is attributable to the diminished electron transfer rate at semiconductor surfaces due to the slightly insulating effect of the organic monolayer.[57]

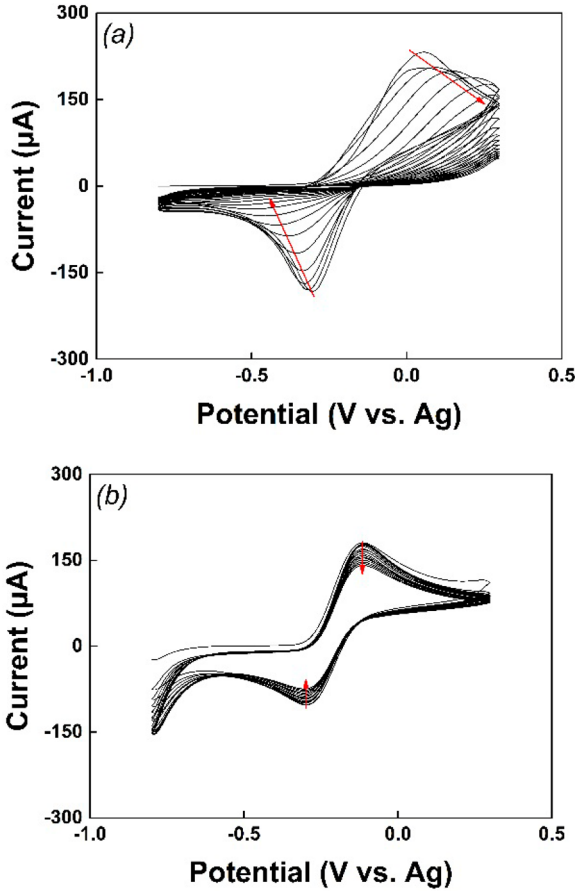

Figure 3. Cyclic voltammograms obtained for Si(111)-**8a**/OH (a) and Si(111)-**8a**/CH_3 (b) surfaces; 30 subsequent scans were performed at a rate of 250 mV s^{-1}. CVs were measured with 2 mM Fc in 1 M $LiClO_4$ in CH_3CN solution at room temperature (ca. 20 °C).

For the Si(111)−**8a**/OH surface, the ΔE_p gradually increased and the current significantly decreased during 30 successive cyclic voltammograms (Figure 3a). This process is likely a result of device degradation due to the formation of surface oxides during anodic corrosion. According to the coverage data, the Si(111)−**8a**/OH (Figure 3a) surface is not sufficiently passivated because of the steric effects of the linker during the functionalization. The incomplete surface functionalization of the Si(111) surface by linker **8a** results in a large proportion of residual Si−Cl sites, which spontaneously oxidize to SiO_x under ambient conditions. This renders the surface susceptible to further hydrolysis and oxidation, which results in an increasingly thick layer of the insulating SiO_x.

In contrast to the Si(111)−**8a**/OH surface (Figure 3a), the ΔE_p value for Si(111)−**8a**/CH_3 (Figure 3b) remains constant over multiple scans despite the applied anodic (and cathodic)

potentials, which indicates that the surface of the Si working electrode remains unchanged during the measurement period (Figure 3b). The small changes in the observed peak current over the 30 consecutive CV scans is simply due to the consumption of ferrocene within the diffusion layer. The original peak current can be re-established upon agitation of the solution, indicating no degradation of the photoelectrode surface. We thus conclude that the small methyl group can infill the unmodified Si sites after functionalization with **8a**, to form a well-packed mixed monolayer on the Si(111) surface.[32] Notably, the cyclic voltammograms for Si(111)−**8a**/CH_3 do show a diminished value of I_{max} (ca. 100 μA) in the reduction current (Figure 3b) as compared to Si(111)−**8a**/OH (ca. 170 μA). This diminished current is likely attributable to the fact that the organic monolayer may function as a small tunneling barrier at the semiconductor/electrolyte interface, thus slowing the electron transfer to the dilute redox species (Fc). Lastly, it is notable that the redox events of Si(111)−**8a**/CH_3 vs Si(111)−**8a**/OH occur at nearly the same potential. This is somewhat unexpected considering the previously documented δ^+ dipole effect induced by the Si−CH_3 unit at Si(111) surfaces.[58] The current comparison suggests that any dipole effect of Si−CH_3 is, to some extent, mimicked by the diamido-triflate linkers. The strong electron withdrawing effect of the aryl triflate moiety may thus simulate some of the electronic properties of the Si−CH_3 unit, although an in-depth study with multiple redox reagents would be required for confirmation of this effect.[58]

Surface Quantification by Covalent Fc Attachment. The ferrocene functionalized samples Si(111)−**8a**/CH_3−Fc and Si(111)−**8c**/CH_3−Fc were subjected to PEC-CV scans (1 sun illumination) with scan rates (ν) ranging from 50 to 2000 mV s^{-1} in 1 M $LiClO_4$ acetonitrile solution. The data are presented in Figure 4a,b, respectively. The observed quasireversible process is attributed to the Fe(II/III) redox cycle of the Heck-coupled ferrocene moiety. Redox peaks between −0.2 and 0 V vs Ag were clearly observed for both samples. Analogous CV measurements on surfaces of **8a**/CH_3 and **8c**/CH_3 without Heck Fc-coupling (and with no redox agent in solution) revealed no significant current (<1 μA). Because there was no ferrocene added to the electrolyte solution, the Faradaic peaks are attributed to the active redox species of vinylferrocene by covalent surface attachment. At a scan rate of 50 mV s^{-1}, the separation of the anodic and cathodic peaks (ΔE_p) are 50 and 42 mV for Si(111)−**8a**/CH_3−Fc and Si(111)−**8c**/CH_3−Fc, respectively. The small ΔE_p illustrates that the rate of interfacial charge transfer is comparable to the voltammetric time scale at slower scan rates. The ΔE_p value increased with increasing scan rate, to 130 mV and 113 mV at a scan rate of 2000 mV s^{-1}, due to the relatively slow interfacial charge transfer compared to the fast scan rate applied to the semiconductor electrode.

The peak current reflects the total number of active redox moieties linked to the working electrode. The smaller peak current for Si(111)−**8c**/CH_3−Fc (Figure 4b) surface as compared to Si(111)−**8c**/CH_3−Fc (Figure 4a) surface corresponds to the lower expected coverage of Fc on the Si(111) surface, as controlled by the larger steric size of **8c**. Analysis of the baseline-corrected peak heights at varying scan rates allows quantification of the total number of redox active ferrocene units covalently attached to the surface. The relationship between anodic peak current (i_p) of Heck-coupling surfaces as a function of scan rate (ν) is shown in Figure 5. For both substrates, i_p increased linearly with ν, which is consistent

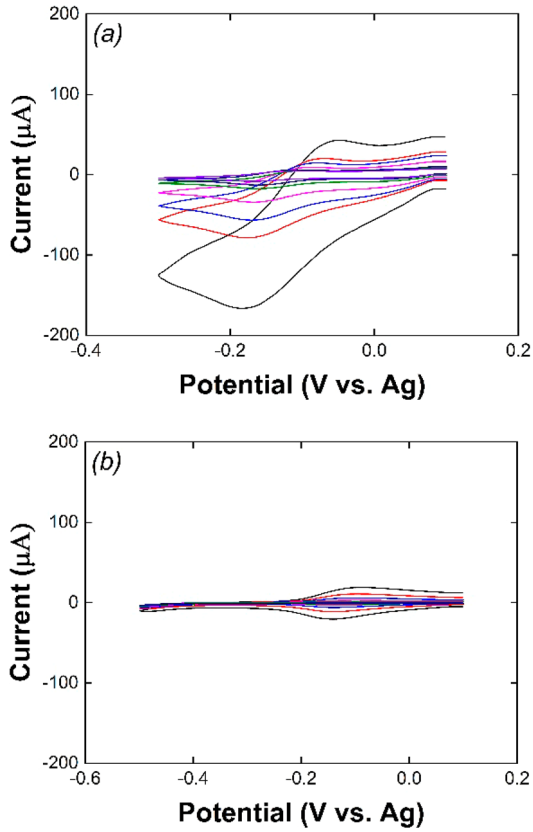

Figure 4. Photoelectrochemical cyclic voltammograms (ν = 50 to 2000 mV s^{-1}) obtained for Si(111) substrates modified with Si(111)−**8a**/CH_3−Fc (a) and Si(111)−**8c**/CH_3−Fc (b) after Heck-coupling reaction with vinylferrocene. Measurements were performed in 1.0 M $LiClO_4$ acetonitrile solution.

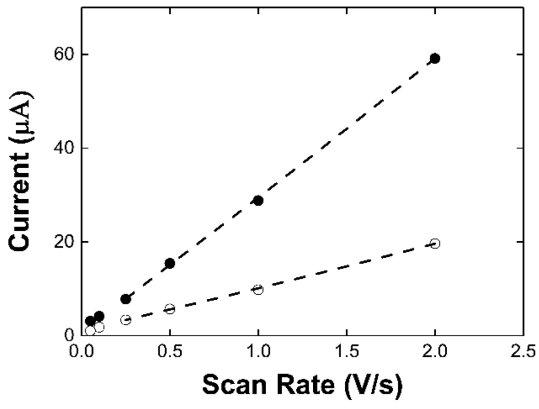

Figure 5. Relationship between i_p and ν obtained from photoelectrodes modified with Si(111)−**8a**/CH_3−Fc (filled circles) and Si(111)−**8c**/CH_3−Fc (open circles) after Heck-coupling reactions with vinylferrocene. CVs of these samples are shown in Figure 4a,b, respectively. Measurements were performed in 1.0 M $LiClO_4$ acetonitrile solution.

with a Faradaic voltammogram for ferrocene moieties chemically bonded to the surface. Thus, the i_p is described by eq 1.

$$i_p = \frac{F^2}{4RT} A\Gamma\nu \quad (1)$$

In this equation, for a one-electron Faradaic reaction, R, T and F are the gas constant, temperature and Faraday's constant,

dx.doi.org/10.1021/am506244m | ACS Appl. Mater. Interfaces 2014, 6, 20557−20568

respectively, and A is the surface area of the working electrode. According to the equation, the surface coverage (Γ) of the ferrocene moieties bonded to the surface can be derived from the slope of the plot in Figure 5. The smaller slope of the Si(111)−**8c**/CH_3−Fc modified surface compared to the Si(111)−**8a**/CH_3−Fc surface reflects the smaller fractional coverage of Fc found with a sterically larger molecular linker.

The electrochemical coverages (Γ) of the covalently functionalized ferrocene surfaces are $5.94 \pm 0.74 \times 10^{-11}$ and $2.39 \pm 0.85 \times 10^{-11}$ mol cm^{-2} for Si(111)−**8a**/CH_3−Fc and Si(111)−**8c**/CH_3−Fc, respectively. Considering the lattice spacing of atop sites on the Si(111) surface (3.84 Å, atop silicon $\sim 1.31 \times 10^{-9}$ mol cm^{-2})[7] the ferrocene coverages are 4.5 ± 0.6% and 1.8 ± 0.7%. Table 1 summarizes the surface coverage calculated from F 1s XPS and also electrochemical measurements. The quantities indicate that the Ferrocene surface coverage varies according to the steric size of the linker. In this series of methylamide linkers with a phenyl core, the most sterically demanding R-group (2-ethylhexyl) requires more space on the surface, thus corresponding to lower surface coverage on both the triflate- and ferrocene-labeled surfaces.

F. XPS Analysis of the Fc-Modified Surface. Lastly, the covalent attachment and quantitative surface coverage of the ferrocene unit was demonstrated by XPS analysis. Figure 6 shows the iron-based 2p XPS signals for Si(111)−**8a**/CH_3−Fc and Si(111)−**8c**/CH_3−Fc surfaces. Formally, the iron center in ferrocene is conventionally assigned as the Fe(II) oxidation state. As shown in Figure 6, one can easily recognize the sharp Fe(II) $2p_{3/2}$ feature at 708.4 eV, with its corresponding 1/2-intensity $2p_{1/2}$ partner near 722 eV. This sharp doublet feature emanates from the highly symmetric ^1A ground state of the low-spin d^6 Fe(II) ion. Also observed is a second set of broader peaks, defined primarily by a broad, weaker intensity Fe(III) $2p_{3/2}$ feature at 712.5 eV, with associated peaks near 715 eV ($2p_{3/2}$ shoulder) and 725 eV ($2p_{1/2}$ main peak and shoulder). This less well-defined set of features derive from the more asymmetric ^2T ground state of the low-spin d^5 Fe(III) ion found in ferrocenium, which exhibits a more complex system of transitions. Thus, the XPS spectrum for each sample exhibited signatures for both Fe(II) and Fe(III) following the Heck-coupling reaction and sample storage. The presence of Fe(III) species in the absence of an applied potential is likely due to charge equilibration between the *n*-type semiconductor and the Fc moiety. As such, the presence of Fe(III) in the XPS spectra could be interpreted as evidence of direct electronic communication between the semiconductor and the covalently attached redox couple.

The Fe(II/III) issue notwithstanding, the corresponding iron-based XPS coverages are 4.2% and 1.4%, respectively, for Si(111)−**8a**/CH_3−Fc and Si(111)−**8c**/CH_3−Fc. The results are consistent with both the fluorine-based XPS coverages as well as the electrochemical quantification mentioned above. Indeed, close inspection of the XPS survey spectra of Si(111)−**8a**/CH_3−Fc and Si(111)−**8c**/CH_3−Fc reveals no detectable F 1s feature (Figures S36 and S38, Supporting Information) after Heck coupling, whereas the F 1s signal is clearly defined in the precursor surfaces Si(111)−**8a**/CH_3 and Si(111)−**8c**/CH_3. This indicates a ~1:1 conversion of the triflate functionality to the vinlyferrocene moiety. It is also noteworthy that very little SiO_x 2p (102 eV) was observed in samples following aerobic transfer from the Heck-coupling reaction to the XPS instrument (see Figures S37 and S39,Supporting Information). This provides further evidence regarding the near-complete passivation of the Si(111)−**8a**/CH_3−Fc surface.

G. Surface Recombination Velocity Measurements. To assess the electronic quality of the surface passivation, the surface recombination velocities were measured. The carrier lifetime decay curves for the functionalized Si(111) substrates are shown in Figure 7, and the lifetimes (τ, μs) and resulting surface recombination velocities (S, cm s^{-1}) are summarized in

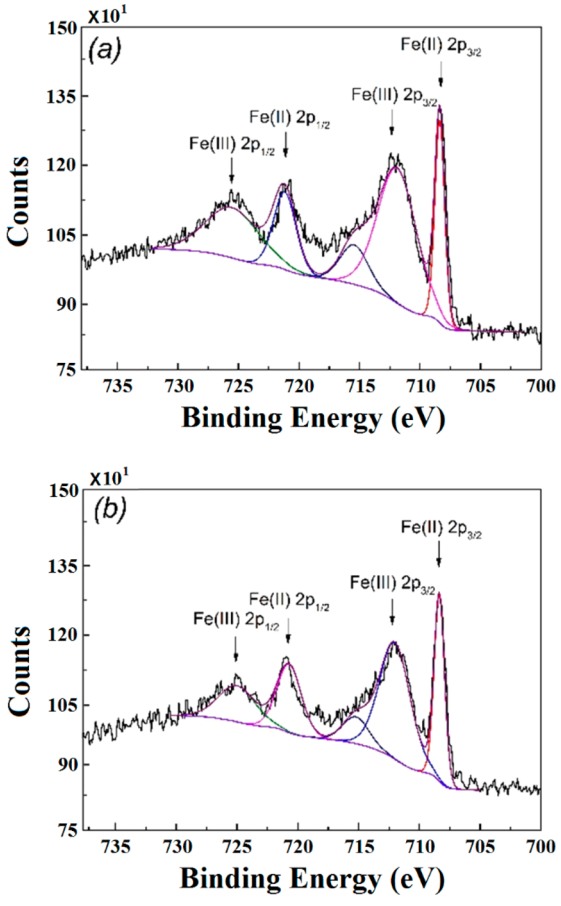

Figure 6. High-resolution Fe 2p XPS spectra for the surfaces Si(111)−**8a**/CH_3−Fc (a, higher coverage) and Si(111)−**8c**/CH_3−Fc (b, lower coverage) after Heck-coupling reaction.

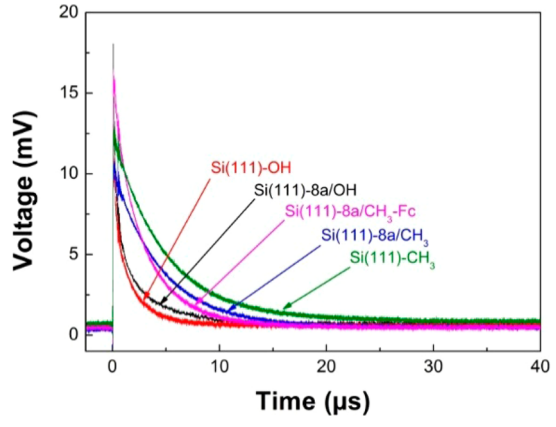

Figure 7. Carrier lifetime decay curves for Si(111)−OH (red), Si(111)−**8a**/OH (black), Si(111)−**8a**/CH_3 (violet), Si(111)−**8a**/CH_3−Fc (blue) and Si(111)−CH_3 (green).

dx.doi.org/10.1021/am506244m | ACS Appl. Mater. Interfaces 2014, 6, 20557−20568

Table 3. As benchmarks, SRV measurements were first performed on both the unpassivated Si(111)−OH surface and the ~100% passivated Si(111)−CH_3 substrate. The Si(111)−OH sample displayed the short surface carrier lifetime, corresponding to an SRV value of S = 11 700 cm s^{-1}. In contrast, the methylated surface Si(111)−CH_3 exhibited a much smaller S value of 3620 cm s^{-1}, approximately 3- to 4-fold slower than the Si(111)−OH substrate. It should be noted that these measurements were performed on the actual substrates used in photo/electrochemical measurements [i.e., *n*-type Si(111); 1−10 Ω·cm], and thus the observed S values are much higher than those reported for intrinsic silicon wafers,[32] which possess very low dopant densities. Nonetheless, the comparative nature of the measurement is a strong indicator of the electronic qualities of the surfaces.

Table 3. Surface Recombination Velocities and Lifetimes for Functionalized Si(111) Surfaces

surface	carrier lifetimes (τ), μs	surface recombination velocity (S), cm s^{-1}
Si(111)−OH	1.49	11700
Si(111)−**8a**/OH	2.12	8260
Si(111)−**8a**/CH_3	4.51	3880
Si(111)−**8a**/CH_3−Fc	3.88	4510
Si(111)−CH_3	4.84	3620

Samples functionalized with the triflate diamide linker **8a** [Si(111)−**8a**/OH] but without methylation exhibited a relatively high surface recombination velocity of S = 8260 cm s^{-1}, which was closest to the unpassivated Si(111)−OH benchmark value of S = 11 600 cm s^{-1}. In contrast, the analogous sample that underwent the methylation procedure, namely Si(111)−**8a**/CH_3, exhibited a relatively low SRV of S = 3880 cm s^{-1}, which is very close to the value of the fully passivated Si(111)−CH_3 sample (S = 3620 cm s^{-1}). These results indicate that the surface coverage of linker **8a** alone is not high enough to provide a large extent of surface passivation. This is consistent with the large steric size of **8a**, which would prevent the linker from occupying each atop site; this is corroborated by the XPS coverage data (**8a**: 6.7 ± 0.8%). Second, the data suggests that the passivation on Si(111)−**8a** is almost completely rescued by the subsequent methylation procedure, which converts the large number of remaining Si−Cl atop sites to Si−CH_3 units. The observed SRV results are consistent with the electrochemical data discussed above (stability and performance, Section E). Specifically, it is noted that the ΔE_p value for the methylated Si(111)−**8a**/CH_3 sample (~200 mV) is less than that of Si(111)−**8a**/CH_3 (~300 mV), indicating that the methylated (i.e., passivated) surface possesses less of a SiO_x barrier layer and less surface defects, and thus exhibits behavior more indicative of an ideal photoelectrode.

Lastly, the SRV measurement was performed on the sample covalently modified with vinylferrocene via the Heck-coupling procedure. The methyl-passivated and Heck-coupled substrate Si(111)−**8a**/CH_3−Fc exhibited relatively high surface carrier lifetimes and a correspondingly low S value of 4510 cm s^{-1} (Table 3), which was closest to that of the methylated substrate [Si(111)−CH_3; 3620 cm s^{-1}]. This indicates that the secondary chemistry to attach the redox marker does not affect the electronic surface quality via the formation of trap states as compared to fully passivated *n*-Si(111)−CH_3 surface. Overall, the SRV results are qualitatively consistent with water contact angle data, XPS measurements and the electrochemistry results, as shown in the previous sections.

CONCLUSION

In this study, we have demonstrated that the surface coverage of phenyl-based molecular linkers can be controlled by synthetically varying the steric size of the R groups at the periphery of the linker. Our results indicate that subsequent methylation results in a linker/CH_3 mixed-monolayer that minimizes unmodified atop sites, which otherwise render the surface susceptible to hydrolysis and oxidation. The addition of chemical functionality at the para position (OTf) by a Heck coupling allows for secondary functionalization of highly passivated Si(111) surfaces (high surface carrier lifetimes, low SRV values). The heteroatom functionalities (N, F, Fe) serve as convenient analytical markers, and PEC measurements confirm the high-fidelity electronic communication between the bulk semiconductor and surface-attached redox agent. Overall, the improved synthetic versatility and enhanced photo/electrochemical stability of these linker-modified Si(111) surfaces will expand the scope of possible devices for PEC applications and catalyst integration in a solar fuels device.

ASSOCIATED CONTENT

Supporting Information

Additional XPS spectra of various Si surfaces, ^{1}H NMR and ^{13}C NMR of compounds **2**, **3**, **4**, **6a−c**, **7a−c** and **8a−c** and mass spectral and IR spectra of compounds **8a−c**. This material is available free of charge via the Internet at http://pubs.acs.org.

AUTHOR INFORMATION

Corresponding Author

*M. J. Rose. E-mail: mrose@cm.utexas.edu.

Notes

The authors declare no competing financial interest.

ACKNOWLEDGMENTS

This research was supported by the U.S. Office of Naval Research (N00014-13-1-0530), the Robert A Welch Foundation (F-1822), the American Chemical Society PRF program (53542-DN13) and the UT Austin College of Natural Sciences. We also acknowledge the National Science Foundation (Grant No. 0618242) for providing the Kratos Axis Ultra XPS used in this work.

REFERENCES

(1) Bansal, A.; Lewis, N. S. Stabilization of Si Photoanodes in Aqueous Electrolytes through Surface Alkylation. *J. Phys. Chem. B* **1998**, *102*, 4058−4060.

(2) Royea, W. J.; Juang, A.; Lewis, N. S. Preparation of Air-Stable, Low Recombination Velocity Si(111) Surfaces Through Alkyl Termination. *Appl. Phys. Lett.* **2000**, *77*, 1988−1990.

(3) Bansal, A.; Li, X. L.; Yi, S. I.; Weinberg, W. H.; Lewis, N. S. Spectroscopic Studies of the Modification of Crystalline Si(111) Surfaces With Covalently-Attached Alkyl Chains Using a Chlorination/Alkylation Method. *J. Phys. Chem. B* **2001**, *105*, 10266−10277.

(4) Webb, L. J.; Lewis, N. S. Comparison of the Electrical Properties and Chemical Stability of Crystalline Silicon(111) Surfaces Alkylated Using Grignard Reagents or Olefins with Lewis Acid Catalysts. *J. Phys. Chem. B* **2003**, *107*, 5404−5412.

(5) Webb, L. J.; Nemanick, E. J.; Biteen, J. S.; Knapp, D. W.; Michalak, D. J.; Traub, M. C.; Chan, A. S. Y.; Brunschwig, B. S.; Lewis, N. S. High-Resolution X-ray Photoelectron Spectroscopic Studies of

Alkylated Silicon(111) Surfaces. *J. Phys. Chem. B* **2005**, *109*, 3930−3937.
(6) Yu, H. B.; Webb, L. J.; Ries, R. S.; Solares, S. D.; Goddard, W. A.; Heath, J. R.; Lewis, N. S. Low-Temperature STM Images of Methyl-Terminated Si(111) Surfaces. *J. Phys. Chem. B* **2005**, *109*, 671−674.
(7) Nemanick, E. J.; Hurley, P. T.; Brunschwig, B. S.; Lewis, N. S. Chemical and Electrical Passivation of Silicon (111) Surfaces through Functionalization with Sterically Hindered Alkyl Groups. *J. Phys. Chem. B* **2006**, *110*, 14800−14808.
(8) Clem, P. G.; Jeon, N. L.; Nuzzo, R. G.; Payne, D. A. Monolayer-Mediated Deposition of Tantalum(V) Oxide Thin Film Structures from Solution Precursors. *J. Am. Ceram. Soc.* **1997**, *80*, 2821−2827.
(9) Srinivasan, U.; Houston, M. R.; Howe, R. T.; Maboudian, R. Alkyltrichlorosilane-based Self-Assembled Monolayer Films for Stiction Reduction in Silicon Micromachines. *J. Microelectromech. Syst.* **1998**, *7*, 252−260.
(10) Ashurst, W. R.; Yau, C.; Carraro, C.; Lee, C.; Kluth, G. J.; Howe, R. T.; Maboudian, R. Alkene based Monolayer Films as Anti-Stiction Coatings for Polysilicon MEMS. *Sens. Actuators, A* **2001**, *91*, 239−248.
(11) Ko, H.; Peleshanko, S.; Tsukruk, V. V. Combing and Bending of Carbon Nanotube Arrays with Confined Microfluidic Flow on Patterned Surfaces. *J. Phys. Chem. B* **2004**, *108*, 4385−4393.
(12) Bansal, A.; Lewis, N. S. Electrochemical Properties of (111)-Oriented n-Si Surfaces Derivatized with Covalently-Attached Alkyl Chains. *J. Phys. Chem. B* **1998**, *102*, 1067−1070.
(13) Lewis, N. S. Frontiers of Research in Photoelectrochemical Solar Energy Conversion. *J. Electroanal. Chem.* **2001**, *508*, 1−10.
(14) Maeda, H.; Sakamoto, R.; Nishimori, Y.; Sendo, J.; Toshimitsu, F.; Yamanoi, Y.; Nishihara, H. Bottom-Up Fabrication of Redox-Active Metal Complex Oligomer Wires on an H-Terminated Si(111) Surface. *Chem. Commun.* **2011**, *47*, 8644−8646.
(15) Yamanoi, Y.; Sendo, J.; Kobayashi, T.; Maeda, H.; Yabusaki, Y.; Miyachi, M.; Sakamoto, R.; Nishihara, H. A New Method To Generate Arene-Terminated Si(111) and Ge(111) Surfaces via a Palladium-Catalyzed Arylation Reaction. *J. Am. Chem. Soc.* **2012**, *134*, 20433−20439.
(16) Parce, J. W.; Owicki, J. C.; Kercso, K. M.; Sigal, G. B.; Wada, H. G.; Muir, V. C.; Bousse, L. J.; Ross, K. L.; Sikic, B. I.; Mcconnell, H. M. Detection of Cell-Affecting Agents with a Silicon Biosensor. *Science* **1989**, *246*, 243−247.
(17) Lin, V. S. Y.; Motesharei, K.; Dancil, K. P. S.; Sailor, M. J.; Ghadiri, M. R. A Porous Silicon-based Optical Interferometric Biosensor. *Science* **1997**, *278*, 840−843.
(18) Strother, T.; Cai, W.; Zhao, X. S.; Hamers, R. J.; Smith, L. M. Synthesis and Characterization of DNA-Modified Silicon (111) Surfaces. *J. Am. Chem. Soc.* **2000**, *122*, 1205−1209.
(19) Bent, S. F. Organic Functionalization of Group IV Semiconductor Surfaces: Principles, Examples, Applications, and Prospects. *Surf. Sci.* **2002**, *500*, 879−903.
(20) Ciampi, S.; Harper, J. B.; Gooding, J. J. Wet Chemical Routes to the Assembly of Organic Monolayers on Silicon Surfaces via the Formation of Si-C Bonds: Surface Preparation, Passivation and Functionalization. *Chem. Soc. Rev.* **2010**, *39*, 2158−2183.
(21) Linford, M. R.; Chidsey, C. E. D. Alkyl Monolayers Covalently Bonded to Silicon Surfaces. *J. Am. Chem. Soc.* **1993**, *115*, 12631−12632.
(22) Tian, F.; Teplyakov, A. V. Silicon Surface Functionalization Targeting Si-N Linkages. *Langmuir* **2013**, *29*, 13−28.
(23) Yablonovitch, E.; Allara, D. L.; Chang, C. C.; Gmitter, T.; Bright, T. B. Unusually Low Surface-Recombination Velocity on Silicon and Germanium Surfaces. *Phys. Rev. Lett.* **1986**, *57*, 249−252.
(24) Tan, M. X.; Lewis, N. S. Charge Transfer Rate Constants for the Reduction of Cobaltocenium at Accumulated n-Si Electrodes. *Inorg. Chim. Acta* **1996**, *242*, 311−321.
(25) Mende, G.; Finster, J.; Flamm, D.; Schulze, D. Oxidation of Etched Silicon in Air at Room-Temperature - Measurements with Ultrasoft X-ray Photoelectron-Spectroscopy (ESCA) and Neutron-Activation Analysis. *Surf. Sci.* **1983**, *128*, 169−175.
(26) Niwano, M.; Kageyama, J.; Kurita, K.; Kinashi, K.; Takahashi, I.; Miyamoto, N. Infrared-Spectroscopy Study of Initial-Stages of Oxidation of Hydrogen-Terminated Si Surfaces Stored in Air. *J. Appl. Phys.* **1994**, *76*, 2157−2163.
(27) Zhang, X.; Garfunkel, E.; Chabal, Y. J.; Christman, S. B.; Chaban, E. E. Stability of HF-Etched Si(100) Surfaces in Oxygen Ambient. *Appl. Phys. Lett.* **2001**, *79*, 4051−4053.
(28) Boukherroub, R.; Morin, S.; Sharpe, P.; Wayner, D. D. M.; Allongue, P. Insights into the Formation Mechanisms of Si-OR Monolayers from the Thermal Reactions of Alcohols and Aldehydes with Si(111)-H. *Langmuir* **2000**, *16*, 7429−7434.
(29) Sano, H.; Maeda, H.; Ichii, T.; Murase, K.; Noda, K.; Matsushige, K.; Sugimura, H. Alkyl and Alkoxyl Monolayers Directly Attached to Silicon: Chemical Durability in Aqueous Solutions. *Langmuir* **2009**, *25*, 5516−5525.
(30) Bansal, A.; Li, X. L.; Lauermann, I.; Lewis, N. S.; Yi, S. I.; Weinberg, W. H. Alkylation of Si Surfaces Using a Two-Step Halogenation Grignard Route. *J. Am. Chem. Soc.* **1996**, *118*, 7225−7226.
(31) Becker, J. S.; Brown, R. D.; Johansson, E.; Lewis, N. S.; Sibener, S. J. Helium Atom Diffraction Measurements of the Surface Structure and Vibrational Dynamics of CH_3-Si(111) and CD_3-Si(111) Surfaces. *J. Chem. Phys.* **2010**, *133*, 104705.
(32) O'Leary, L. E.; Rose, M. J.; Ding, T. X.; Johansson, E.; Brunschwig, B. S.; Lewis, N. S. Heck Coupling of Olefins to Mixed Methyl/Thienyl Monolayers on Si(111) Surfaces. *J. Am. Chem. Soc.* **2013**, *135*, 10081−10090.
(33) Moore, G. F.; Sharp, I. D. A Noble-Metal-Free Hydrogen Evolution Catalyst Grafted to Visible Light-Absorbing Semiconductors. *J. Phys. Chem. Lett.* **2013**, *4*, 568−572.
(34) He, J.; Patitsas, S. N.; Preston, K. F.; Wolkow, R. A.; Wayner, D. D. M. Covalent Bonding of Thiophenes to Si(111) by a Halogenation/Thienylation Route. *Chem. Phys. Lett.* **1998**, *286*, 508−514.
(35) Bergerson, W. F.; Mulder, J. A.; Hsung, R. P.; Zhu, X. Y. Assembly of Organic Molecules on Silicon Surfaces via the Si-N Linkage. *J. Am. Chem. Soc.* **1999**, *121*, 454−455.
(36) Tian, F. Y.; Taber, D. F.; Teplyakov, A. V. -NH- Termination of the Si(111) Surface by Wet Chemistry. *J. Am. Chem. Soc.* **2011**, *133*, 20769−20777.
(37) Buriak, J. M. Organometallic Chemistry on Silicon Surfaces: Formation of Functional Monolayers Bound Through Si-C Bonds. *Chem. Commun.* **1999**, 1051−1060.
(38) Liu, Y.; Yamazaki, S.; Yamabe, S.; Nakato, Y. A Mild and Efficient Si(111) Surface Modification via Hydrosilylation of Activated Alkynes. *J. Mater. Chem.* **2005**, *15*, 4906−4913.
(39) Tajimi, N.; Sano, H.; Murase, K.; Lee, K. H.; Sugimura, H. Thermal Immobilization of Ferrocene Derivatives on (111) Surface of n-Type Silicon: Parallel Between Vinylferrocene and Ferrocenecarboxaldehyde. *Langmuir* **2007**, *23*, 3193−3198.
(40) Ciampi, S.; Eggers, P. K.; Le Saux, G.; James, M.; Harper, J. B.; Gooding, J. J. Silicon (100) Electrodes Resistant to Oxidation in Aqueous Solutions: An Unexpected Benefit of Surface Acetylene Moieties. *Langmuir* **2009**, *25*, 2530−2539.
(41) Okada, R.; Miyadera, T.; Shimada, T.; Koma, A.; Ueno, K.; Saiki, K. Methyl-Terminated Si(111) Surface as the Ultra Thin Protection Layer to Fabricate Position-Controlled Alkyl SAMs by Using Atomic Force Microscope Anodic Oxidation. *Surf. Sci.* **2004**, *552*, 46−52.
(42) Nielander, A. C.; Bierman, M. J.; Petrone, N.; Strandwitz, N. C.; Ardo, S.; Yang, F.; Hone, J.; Lewis, N. S. Photoelectrochemical Behavior of n-Type Si(111) Electrodes Coated with a Single Layer of Graphene. *J. Am. Chem. Soc.* **2013**, *135*, 17246−17249.
(43) Bolts, J. M.; Bocarsly, A. B.; Palazzotto, M. C.; Walton, E. G.; Lewis, N. S.; Wrighton, M. S. Chemically Derivatized N-Type Silicon Photoelectrodes - Stabilization to Surface Corrosion in Aqueous-Electrolyte Solutions and Mediation of Oxidation Reactions by Surface-Attached Electroactive Ferrocene Reagents. *J. Am. Chem. Soc.* **1979**, *101*, 1378−1385.

(44) Buriak, J. M. Organometallic Chemistry on Silicon and Germanium Surfaces. *Chem. Rev.* **2002**, *102*, 1271−1308.
(45) Wayner, D. D. M.; Wolkow, R. A. Organic Modification of Hydrogen Terminated Silicon Surfaces. *J. Chem. Soc., Perkin Trans. 2* **2002**, 23−34.
(46) Ciampi, S.; Harper, J. B.; Gooding, J. J. Wet Chemical Routes to the Assembly of Organic Monolayers on Silicon Surfaces via the Formation of Si-C Bonds: Surface Preparation, Passivation and Functionalization. *Chem. Soc. Rev.* **2010**, *39*, 2158−2183.
(47) Rohde, R. D.; Agnew, H. D.; Yeo, W. S.; Bailey, R. C.; Heath, J. R. A Non-Oxidative Approach Toward Chemically and Electrochemically Functionalizing Si(111). *J. Am. Chem. Soc.* **2006**, *128*, 9518−9525.
(48) O'Leary, L. E.; Johansson, E.; Brunschwig, B. S.; Lewis, N. S. Synthesis and Characterization of Mixed Methyl/Allyl Monolayers on Si(111). *J. Phys. Chem. B* **2010**, *114*, 14298−14302.
(49) Johansson, E.; Boettcher, S. W.; O'Leary, L. E.; Poletayev, A. D.; Maldonado, S.; Brunschwig, B. S.; Lewis, N. S. Control of the pH-Dependence of the Band Edges of Si(111) Surfaces Using Mixed Methyl/Allyl Monolayers. *J. Phys. Chem. C* **2011**, *115*, 8594−8601.
(50) Nemanick, E. J.; Hurley, P. T.; Webb, L. J.; Knapp, D. W.; Michalak, D. J.; Brunschwig, B. S.; Lewis, N. S. Chemical and Electrical Passivation of Single-Crystal Silicon(100) Surfaces Through a Two-Step Chlorination/Alkylation Process. *J. Phys. Chem. B* **2006**, *110*, 14770−14778.
(51) Perring, M.; Dutta, S.; Arafat, S.; Mitchell, M.; Kenis, P. J.; Bowden, N. B. Simple Methods for the Direct Assembly, Functionalization, and Patterning of Acid-Terminated Monolayers on Si(111). *Langmuir* **2005**, *21*, 10537−10544.
(52) Kaku, T.; Matsunaga, N.; Ojida, A.; Tanaka, T.; Hara, T.; Yamaoka, M.; Kusaka, M.; Tasaka, A. 17,20-Lyase Inhibitors. Part 4: Design, Synthesis and Structure-Activity Relationships of Naphthylmethylimidazole Derivatives as Novel 17,20-Lyase Inhibitors. *Bioorg. Med. Chem.* **2011**, *19*, 1751−1770.
(53) Perring, M.; Dutta, S.; Arafat, S.; Mitchell, M.; Kenis, P. J. A.; Bowden, N. B. Simple Methods for the Direct Assembly, Functionalization, and Patterning of Acid-Terminated Monolayers on Si(111). *Langmuir* **2005**, *21*, 10537−10544.
(54) Bodlaki, D.; Borguet, E. Photoreactivity of Si(111)-H in Ambient. *J. Phys. Chem. C* **2007**, *111*, 234−239.
(55) Linford, M. R.; Fenter, P.; Eisenberger, P. M.; Chidsey, C. E. D. Alkyl Monolayers on Silicon Prepared from 1-Alkenes and Hydrogen-Terminated Silicon. *J. Am. Chem. Soc.* **1995**, *117*, 3145−3155.
(56) Zhang, L. Z.; Li, L. Y.; Chen, S. F.; Jiang, S. Y. Measurements of Friction and Adhesion for Alkyl Monolayers on Si(111) by Scanning Force Microscopy. *Langmuir* **2002**, *18*, 5448−5456.
(57) Barrelet, C. J.; Robinson, D. B.; Cheng, J.; Hunt, T. P.; Quate, C. F.; Chidsey, C. E. D. Surface Characterization and Electrochemical Properties of Alkyl, Fluorinated Alkyl, and Alkoxy Monolayers on Silicon. *Langmuir* **2001**, *17*, 3460−3465.
(58) Grimm, R. L.; Bierman, M. J.; O'Leary, L. E.; Strandwitz, N. C.; Brunschwig, B. S.; Lewis, N. S. Comparison of the Photoelectrochemical Behavior of H-Terminated and Methyl-Terminated Si(111) Surfaces in Contact with a Series of One-Electron, Outer-Sphere Redox Couples in CH_3CN. *J. Phys. Chem. C* **2012**, *116*, 23569−23576.